GPR55 controls functional differentiation of self-renewing epithelial progenitors for salivation

Solomiia Korchynska,[1] **Mirjam I. Lutz,**[2] **Erzsébet Borók,**[1,3] **Johannes Pammer,**[4] **Valentina Cinquina,**[1] **Nataliya Fedirko,**[5] **Andrew J. Irving,**[6] **Ken Mackie,**[7] **Tibor Harkany,**[1,8] **and Erik Keimpema**[1]

[1]Department of Molecular Neurosciences, Center for Brain Research, [2]Institute of Neurology, [3]Department of Cognitive Neurobiology, Centre for Brain Research, and [4]Department of Pathology, Medical University of Vienna, Vienna, Austria. [5]Department of Human and Animal Physiology, Biological Faculty, Ivan Franko National University of Lviv, Lviv, Ukraine. [6]School of Biomolecular and Biomedical Science, Conway Institute, University College Dublin, Dublin, Ireland. [7]Gill Center for Biomolecular Sciences, Department of Psychological and Brain Sciences, Indiana University, Bloomington, Indiana, USA. [8]Department of Neuroscience, Karolinska Institutet, Stockholm, Sweden.

GPR55, a lipid-sensing receptor, is implicated in cell cycle control, malignant cell mobilization, and tissue invasion in cancer. However, a physiological role for GPR55 is virtually unknown for any tissue type. Here, we localize GPR55 to self-renewing ductal epithelial cells and their terminally differentiated progeny in both human and mouse salivary glands. Moreover, we find GPR55 expression downregulated in salivary gland mucoepidermoid carcinomas and GPR55 reinstatement by antitumor irradiation, suggesting that GPR55 controls renegade proliferation. Indeed, GPR55 antagonism increases cell proliferation and function determination in quasiphysiological systems. In addition, $Gpr55^{-/-}$ mice present ~50% enlarged submandibular glands with many more granulated ducts, as well as disordered endoplasmic reticuli and with glycoprotein content. Next, we hypothesized that GPR55 could also modulate salivation and glycoprotein content by entraining differentiated excretory progeny. Accordingly, GPR55 activation facilitated glycoprotein release by itself, inducing low-amplitude Ca^{2+} oscillations, as well as enhancing acetylcholine-induced Ca^{2+} responses. Topical application of GPR55 agonists, which are ineffective in $Gpr55^{-/-}$ mice, into adult rodent submandibular glands increased salivation and saliva glycoprotein content. Overall, we propose that GPR55 signaling in epithelial cells ensures both the life-long renewal of ductal cells and the continuous availability of saliva and glycoproteins for oral health and food intake.

Introduction

Salivation is a continuous process indispensable for digestion, taste perception, and oral health. To provide the organism with a constant stream of saliva, mammalian salivary glands are metabolically active throughout life, with saliva produced by luminal cells in serous and mucous acini (contributing watery and mucous-rich excretions, respectively). Saliva then flows sequentially along intercalated, striated, and excretory ducts to reach the oral cavity (Supplemental Figure 1; supplemental material available online with this article; https://doi.org/10.1172/jci.insight.122947DS1). Safeguarding its incessant need to produce saliva, renewal of adult functionally competent ductal and acinar cells is broadly thought to occur through an epithelial stem cell–dependent mechanism, with daughter cells of multipotent progenitors lining intercalated ducts to replace terminally differentiated striated duct and acinar cells (1, 2). While salivary ducts indeed contain their own abluminal epithelial stem cell niche (3), capable of self-renewal (4) and dependent on Wnt/β-catenin signaling (5), recent clonal analysis revealed that differentiated acinar cells themselves might also be able to self-renew (6). Although the contribution of neural afferents to the control of cell renewal in salivary glands during adulthood is less clear, developmental studies on salivary gland organogenesis demonstrate that acetylcholine (ACh) released from parasympathetic nerves is necessary to promote abluminal epithelial progenitor cell proliferation and differentiation in an M1/M3 muscarinic receptor and epidermal growth factor–dependent mechanism (7). Accordingly, parasympathectomy in the adult halves salivary gland regeneration (8), reinforcing that ACh released from parasympathetic nerves

is mandatory for tissue size control by instructing self-renewing tissue-resident progenitors. Nevertheless, whether cell-autonomous and tissue-specific signal amplification steps exist, coordinate, and diversify ACh effects on secretory ductal cells remain unknown.

We sought to bridge this gap of knowledge by exploring the signaling contributions of the orphan GPCR 55 (GPR55) (9), a lipid-sensing receptor highly enriched in self-renewing organs, including liver, spleen, and salivary glands of many mammals, such as humans (10). GPR55 signaling has predominantly been studied in pathologies associated with errant cell cycle control, such as obesity (11) and cancer (12–14). In the latter, GPR55 signaling promotes cancer invasion (15, 16) and directional cell migration (10). Available data also suggest a positive correlation between expression levels of GPR55 and metabolic enzymes for L-α-lysophosphatidylinositol (LPI), its endogenous ligand (17), and its tumor growth, invasiveness (18, 19), and negative prognosis for survival (20). However, evidence for GPR55 signaling in physiological contexts in any organ system is lacking beyond the LPI-induced inhibition of the differentiation of bone macrophages (21) and glucose-induced insulin secretion from pancreatic β cells (22). Here, we focused on cell fate- and function-determination by GPR55 in salivary glands because (a) bulk tissue mRNA analysis assigns GPR55 expression to salivary glands in humans (10) and (b) salivary regeneration from tissue-resident progenitors is appealing to treat xerostomia (dry mouth syndrome) upon gland degeneration in, for example, Sjögren's syndrome or after radiation therapy–induced tissue damage (23). Moreover, the spatial proximity of tissue-specific progenitors and differentiated excretory progenies calls for the existence of dual-acting signaling systems that, irrespective of being either cell-autonomous or paracrine, can control organ size to ideally fit physiological requirements of salivation.

Here, we first defined the cellular localization of GPR55 at the mRNA and protein levels in both human and mouse submandibular and parotid salivary glands, and we found that it expressed mainly in striated ducts and myoepithelial cells, with its localization to intercalated ducts being specific to human tissues. Since GPR55 was found on ductal abluminal cells capable of self-renew (3), we hypothesized that GPR55 signaling might modulate the turnover of ductal progenitors. Therefore, we examined GPR55 expression in human mucoepidermoid carcinomas, thought to be derived from proliferating abluminal stem cells (24), and found GPR55 levels to be decreased. Strikingly, GPR55 was significantly increased in therapeutically irradiated tissues, which coincides with reduced cell proliferation, signifying successful radiation therapy (23). We recapitulated these findings in cultured salispheres by pharmacological inhibition of GPR55, resulting in significantly increased salisphere size and proliferation rates. Furthermore, genetic deletion of *Gpr55* in mice resulted in distended glands with enlarged granulated ducts, as well as significant hyperproliferation in both male and female *Gpr55*$^{-/-}$ submandibular glands. As such, GPR55 antagonism promoted cellular maturation and increased glycoprotein content in differentiated progeny of *Gpr55*$^+$ epithelial progenitors. Conspicuously, we also observed strongly distorted endoplasmic reticuli compressed by sequestered glycoprotein in *Gpr55*$^{-/-}$ mice, suggestive of impaired saliva release. Indeed, LPI induces Ca^{2+} signaling in cultured salispheres to amplify prosecretory cholinergic stimuli. Accordingly, injection of the synthetic GPR55 agonist *N*-([4-(*N*-Phenylsulfamoyl)phenylcarbamothioyl]-[1,1′-biphenyl]-4-carboxamide) (N-PCC) (25) into submandibular glands significantly increased the rate of salivation and glycoprotein content of the outflow, showcasing GPR55's on-demand contribution to salivation. We propose that GPR55 signaling acts as a cell-specific gatekeeper by enhancing ACh-induced salivation and simultaneously limiting ACh-induced cell proliferation, thus precisely matching salivary cell-pool size to functional output throughout life.

Results

GPR55 expression in human and mouse salivary glands. In humans, GPR55 mRNA has been detected in a variety of self-renewing tissues, including the salivary gland (10), but its subcellular localization remains unknown. Here, we first performed in situ hybridization for *Gpr55* mRNA in the human submandibular gland, a mixed gland (serous and mucous acini) that produces the majority of saliva (Figure 1A and Supplemental Figure 1A). We found significant *Gpr55* mRNA expression in myoepithelial cells flanking mucous acini but not in serous and mucous acinar cells. Luminal cells of intercalated ducts also contained a pronounced *Gpr55* mRNA signal (Figure 1A), with low levels observed in luminal cells of striated ducts. IHC using newly developed reagents (for antibody characterization, including controls; Figure 2, A–F) detected GPR55 protein primarily in intercalated and striated ducts (luminar and abluminar cells), with lower amounts in myoepithelial cells and serous acini but not mucous acini (Figure 1B and Supplemental Figure 2A).

Even though GPR55 protein was found in submandibular serous acini, we noted significant tissue variability, given its nearly complete absence in serous acini of the parotid gland (Supplemental Figure 2B). Strikingly, immunolabeling for Ca^{2+}-dependent phospholipase A2 (PLA2G4A), a member of the PLA2 superfamily converting phosphatidylinositol (PI) to GPR55's endogenous ligand LPI (26, 27), revealed perinuclear PLA-2G4A distribution to coincide with GPR55 in striated and intercalated ducts, as well as serous and demilune acinar cells (half-moon–shaped serous acini) in submandibular glands (Figure 1C). These data suggest the possible existence of autocrine and/or short-range paracrine LPI-GPR55 signaling in or among cells with self-renewing capacity (14).

In mice, quantitative PCR (qPCR) data (Figure 1D and Supplemental Figure 1B) combined with in situ hybridization revealed GPR55 mRNA predominantly in convoluted granular ducts and intercalated ducts. Fluorescence IHC assigned GPR55 protein predominantly to granulated ducts of the submandibular gland, with minute signaling in striated ducts and its complete absence in acini (Figure 1E and Supplemental Figure 2C). Even though we also detected GPR55-like immunoreactivity in striated ducts, this was deemed unspecific because of its retention in $Gpr55^{-/-}$ tissues (Figure 2D). In granular duct cells, GPR55 was found concentrated proximal to nuclei, suggesting enrichment on the ER, as well as on plasma membranes (Figure 1, E and F). These findings cumulatively suggest rapid GPR55 turnover. ER localization was confirmed by the coexistence of GPR55 and protein disulfide-isomerase (PDI), a periplasmic ER enzyme (28) (Supplemental Figure 2, F and G). GPR55 immunoreactivity in the mouse parotid and sublingual glands was limited to striated ducts, mostly appearing somatic, although much weaker than in granulated ducts of the submandibular gland (Figure 1G and Figure 2, E and F). Reminiscent to our findings in humans, PLA2G4A was also perinuclear in appearance in submandibular granular cells, as well as in parotid and sublingual striated duct cells (Figure 1G and Supplemental Figure 3).

GPR55 expression is reduced in salivary gland carcinomas and reinstated by radiotherapy. GPR55 and LPI levels are viewed as predictors of tumor growth and invasiveness. Their increases generally associate with negative outcomes, particularly in carcinomas (12, 18). Since we find GPR55 expressed in self-renewing cell lineages, we asked if GPR55 expression is altered in human salivary gland carcinomas (Supplemental Figure 4, A and B), used as proof-of-concept to implicate GPR55 in cell cycle deregulation. We first semi-quantitatively determined GPR55 protein expression in striated/intercalated ducts and serous acini of the healthy human parotid gland, and we compared these with tissues from epithelial-myoepithelial and muco-epidermoid carcinomas ($n = 5$ cases/carcinoma), as submandibular tumors are rare (Figure 3, A and B). Since carcinoma cells are derived from abluminal ductal stem cells (29), we primarily compared GPR55-like immunoreactivity in ductal structures. In epithelial-myoepithelial carcinomas, GPR55-like immunoreactivity was found at significantly lower levels, as compared with healthy surrounding tissues (Figure 3, A and C). Similarly, in mucoepidermoid carcinomas, GPR55-like immunoreactivity was found at low-to-medium levels (Figure 3, B and C), with quantitative analysis pointing to a significant reduction in GPR55 levels indiscriminately within the tumor mass, as compared with nonaffected sister tissues (Figure 3D).

We hypothesized that, if GPR55 levels are lower in carcinomas to promote renegade proliferation, then radiotherapy — which irreversibly and indiscriminately damages cancer cells and surrounding healthy tissue — would reinstate GPR55 if this receptor contributes to reducing proliferative capacity. Relative to healthy control samples ($n = 5$), and even if presenting a loss of acini, irradiated submandibular glands that no longer contained tumor mass ($n = 5$) showed elevated GPR55-like immunoreactivity with intercalated ducts, and occasionally striated ducts, being strongly immunoreactive (Figure 3, E and F, and Supplemental Figure 4C). Collectively, our data suggest that, instead of only being a biomarker of tumorigenesis, GPR55 might act as a signaling node to limit cell proliferation under physiological conditions, which is switched off in carcinomas (23).

GPR55 activity inhibits cell proliferation in cultured salispheres. If GPR55 signaling is causal to cell renewal, then its pharmacological modulation could be expected to modulate submandibular gland size (Figure 4A). Here, we established mouse submandibular salivary gland cultures (termed salispheres) from *tau2*-EGFP mice (30), harboring EGFP in mature granulated duct cells, with Matrigel embedding for prolonged survival and clonal expansion (Figure 4B). Both $EGFP^+$ and $EGFP^-$ cells expressed GPR55 in size-restricted salispheres (20–40 μm each) from 2 days in vitro onward (Supplemental Figure 5A), which appeared consistent with intracellular (likely ER) localization. We then confirmed that GPR55s were functional by dye imaging with Tocrifluor T1117 (1 μM), a fluorescent lipophilic AM 251 analogue with agonist-like activity at GPR55 (31). Short-term exposure (up to 15 minutes) to T1117 did not result in detectable accumulation
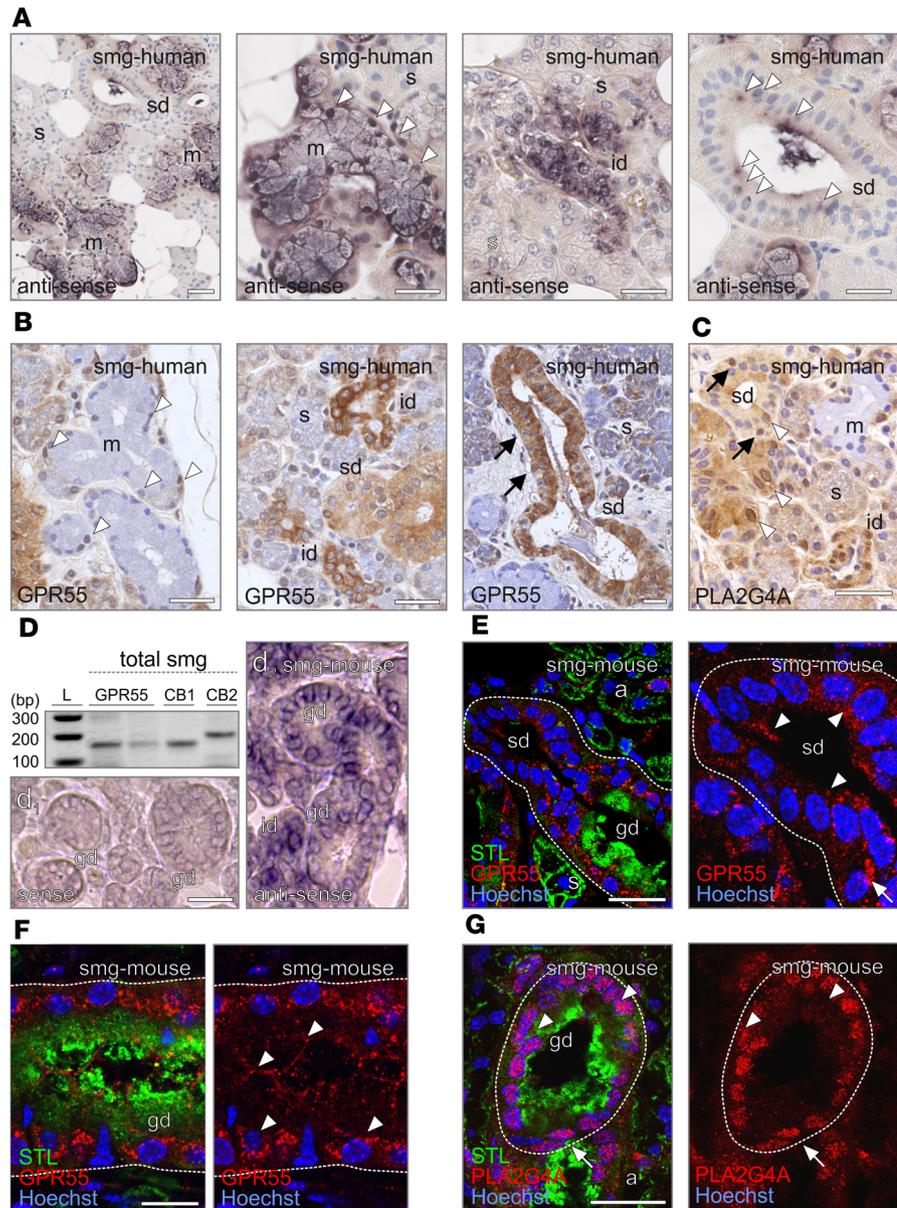
Figure 1. GPR55 distribution in human and mouse salivary glands. (**A**) GPR55 in situ hybridization in human submandibular gland (smg). Signal was observed in myoepithelial cells, intercalated ducts (id), and weakly in striated ducts (sd) but not serous (s) and mucous acini (m). Solid arrowheads point to myoepithelial cells in R_1R and positive in situ signal. (**B**) GPR55 protein expression in human submandibular gland shows weak staining in myoeptithelial cells and serous acini, moderate staining in striated ducts, and strong staining in intercalated ducts. Arrowheads point to myoepithelial cells. Black arrows indicate proliferative abluminal cells. (**C**) PLA2G4A staining in human submandibular gland. Black arrows point to abluminal cell, while white arrowheads indicate luminal cells. (**D**) Mouse submandibular qPCR and in situ hybridization. Signal was detected in intercalated ducts (id), as well as granulated ducts (gd). Acini were mostly negative. Note that the mouse submandibular gland does not have mucous acini. (**E** and **F**) GPR55 protein localization in mouse submandibular gland confirms expression in granulated ducts and striated ducts, but not in acini (a). Granulated ducts were visualized with solanum tuberosum lectin (STL), labeling glycoprotein. Arrowheads point to positive cells and membranes, while arrows indicate abluminal cells. (**G**) PLA2G4A was found mainly in nuclei of granulated ducts (arrowheads). Arrows point to possible myoepithelial cells. Scale bars: 50 μm.
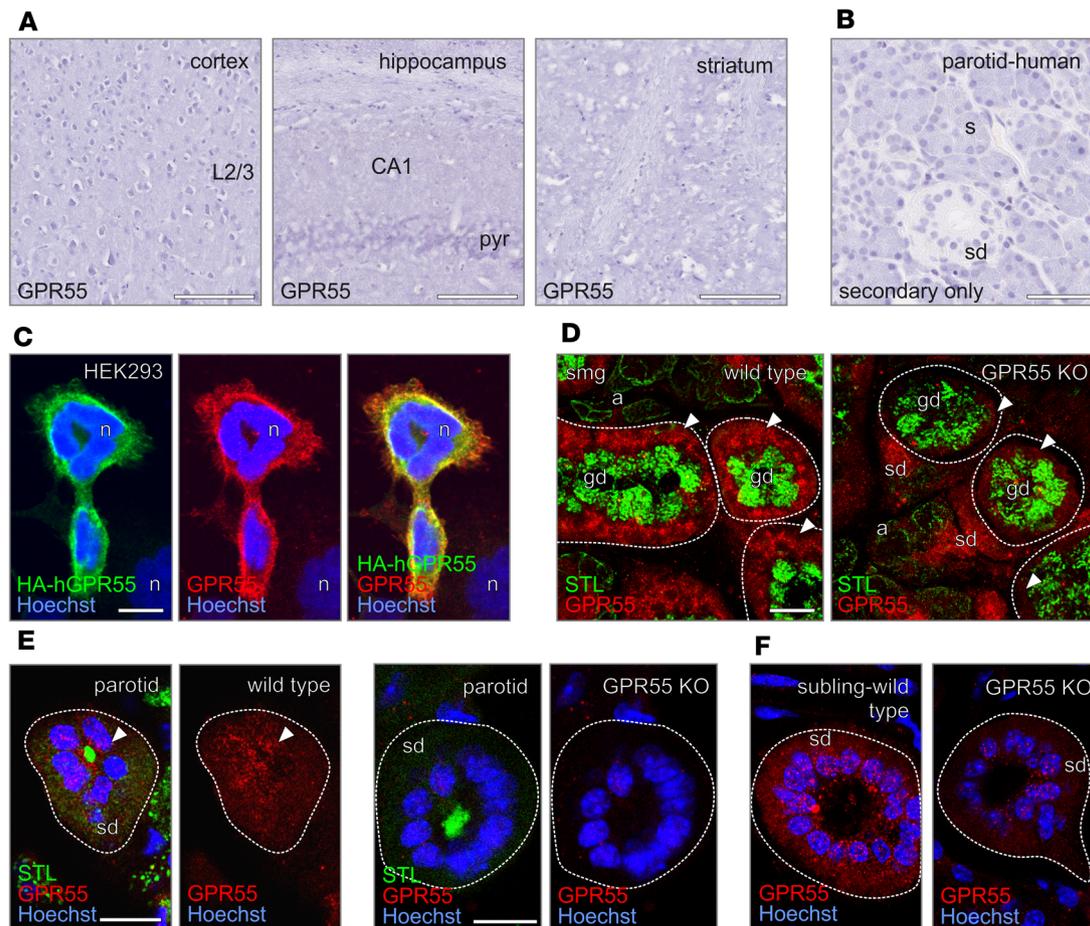
Figure 2. Validation of anti-GPR55 antibodies. (**A**) GPR55 staining in the mouse cortex, hippocampus, and striatum, known to lack appreciable *Gpr55* mRNA expression, reveals no immunoreactivity with our GPR55 antibody. (**B**) Secondary-only antibody control in human parotid gland. (**C**) Colabeling between our GPR55 antibody and the HA-tagged hGPR55 in transfected HEK293 cells. Note that nontransfected cells were not stained by our antibody. (**D–F**) Cellular distribution of GPR55 in *Gpr55*$^{-/-}$ and WT submandibular (**D**), parotid (**E**), and sublingual gland (**F**). Note that granulated ducts are specifically stained in submandibular glands, but there is residual staining in striated ducts of both submandibular and sublingual glands. a, acini; CA1, cornu ammonis 1; gd, granulated duct; id, intercalated duct; L, layer; pyr, pyramidal layer; s, serous acini; sd striated duct. Scale bars: 75 μm (**B**), 50 μm (**A**), 25 μm (**D**, **E**, and **F**), and 10 μm (**C**).

of fluorescent signal. In turn, 1-hour exposure led to the significant cytoplasmic build-up of T1117 fluorescence, as compared with vehicle-treated salispheres (Figure 4C), suggesting that T1117 was either internalized through plasmalemmal GPR55 receptors or could bind intracellular receptors.

Next, we asked if CID 16020046, a GPR55 antagonist (32, 33), enhances cell proliferation in size-restricted salispheres. Exposing salispheres to CID 16020046 (1 μM) for 6 days induced significant cellular expansion, as measured by the number of Hoechst$^+$ nuclei, as compared with vehicle-treated controls (Figure 4D). EdU incorporation confirmed significantly increased cell proliferation, after pulsing EdU for 12 hours at the onset of CID 16020046 stimulation (Figure 4D). Conversely, exposure to GPR55's endogenous agonist LPI (1 μM) or the synthetic agonist N-PCC (100 nM) significantly decreased salisphere size and, simultaneously, EdU incorporation (Figure 4D). Pretreatment with CID 16020046 for 20 minutes was sufficient to overcome LPI- and N-PCC–induced growth restriction (Figure 4D).

Genetic GPR55 inactivation increases salivary gland size and function in vivo. If GPR55 signaling limits submandibular gland size, then mice constitutively lacking *Gpr55* (34) could be expected to carry a salivary gland phenotype. Upon extracting *Gpr55*$^{-/-}$ submandibular glands, the largest of all salivary glands, we first noted their increased size, as compared with WT controls (Figure 5A). H&E staining showed a particularly significant increase in granulated duct surface size in male *Gpr55*$^{-/-}$ animals (Figure 5, B and C), which is compatible with excessive gland growth upon *Gpr55* ablation. Female *Gpr55*$^{-/-}$ mice exhibited similar alterations even with the notion that female submandibular glands are smaller per se than those of male mice
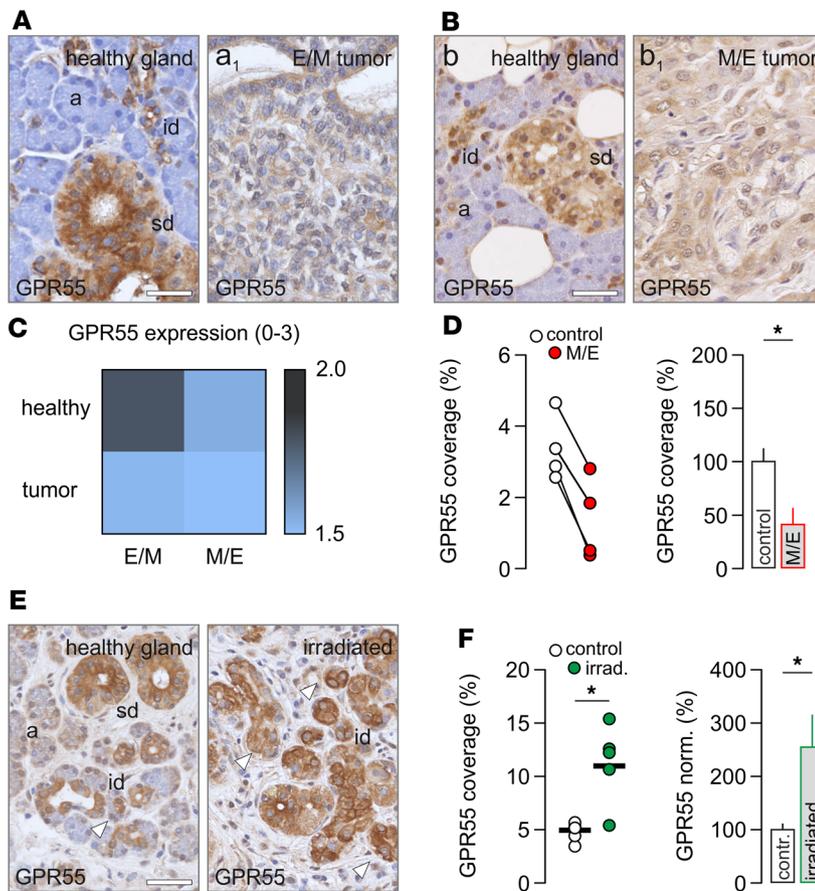
Figure 3. GPR55 is downregulated upon tumorigenic transformation. (A and B). GPR55 expression in epithelial-myoepithelial carcinomas (E/M, $n = 5$) and mucoepidermoid carcinomas (M/E, $n = 5$) of the parotid gland. Note that GPR55 signal is mainly expressed in healthy intercalated (id) and striated ducts (sd) but not serous acini (a), while – in cancer tissues – GPR55 is expressed only at minute levels. (**C**) Heatmap of GPR55 area coverage. A relative scale of 0–3 was used to score GPR55 immunoreactivity. (**D**) In mucoepidermoid carcinomas, tumor tissues express significantly less GPR55 (Student's t test). (**E** and **F**) Irradiation of salivary gland tissue ($n = 5$, Student's t test) increased GPR55 levels in intercalated and striated ducts. Scale bars: 50 μm. Data were expressed as means ± SEM. *$P < 0.05$.

(Supplemental Figure 5B). We hypothesized that increased granular duct size could be either due to cellular enlargement or accelerated replenishment of ductal cells for which GPR55 would otherwise physiologically inhibit renewal (7, 8).

We sought to address if increased cell proliferation accounts for salivary gland enlargement in $Gpr55^{-/-}$ mice by immunostaining for Ki67, a marker of cell proliferation (35), and we found significantly increased density/number of Ki67+ nuclei per granulated duct in $Gpr55^{-/-}$ mice of both sexes relative to WT littermates (Figure 5, D and E, and Supplemental Figure 5, E–H). In addition, quantification of epithelial progenitor markers, such as SOX2 and SOX10 (36), members of the SRY-box family of transcription factors, revealed significant increases in immunoreactive nuclei in the submandibular and parotid gland of $Gpr55^{-/-}$ mice, suggesting life-long excess in cell proliferation (Figure 5, F and G). Cleaved caspase-3+ cells, marking apoptosis (37), showed no significant difference between $Gpr55^{-/-}$ and WT mice (data not shown), making the contribution of disproportionate death rates to the salivary gland phenotype unlikely.

Because GPR55 deletion leads to hyperproliferation and enlarged glands, we posited that gland function could be affected, too. Therefore, we collected saliva from WT and $Gpr55^{-/-}$ mice ($n = 9$; Figure 6A) and quantified saliva flow rate and protein concentration. While base saliva flow rate was unchanged in $Gpr55^{-/-}$ mice relative to WTs, protein concentration determined by Nanodrop measurements was significantly elevated (Figure 6B). Analysis of glycoprotein distribution by the standard periodic acid-Schiff (PAS) reaction confirmed excess glycoprotein storage in $Gpr55^{-/-}$ granular duct cells (Figure 6C and Supplemental Figure 5C). $Gpr55^{-/-}$ ductal cells showed enlarged apical compartments with excess glycoprotein content (Figure 6D and Supplemental Figure 5C), whereas basal compartments shrunk and contained disorganized ER that resided around their nuclei. This anatomical arrangement supports increased glycoprotein synthesis (38) and intracellular storage.

Thereafter, we more specifically probed the basal compartment containing the nucleus and ER, the latter marked by ER protein 29 (ERp29) (39). This showed greatly reduced ER with a coincident shift toward increased apical compartments in both male and female $Gpr55^{-/-}$ ductal cells (Figure 6E and Supplemental Figure 5D), as determined by surface area profiling (Figure 6E). These data confirm that, even
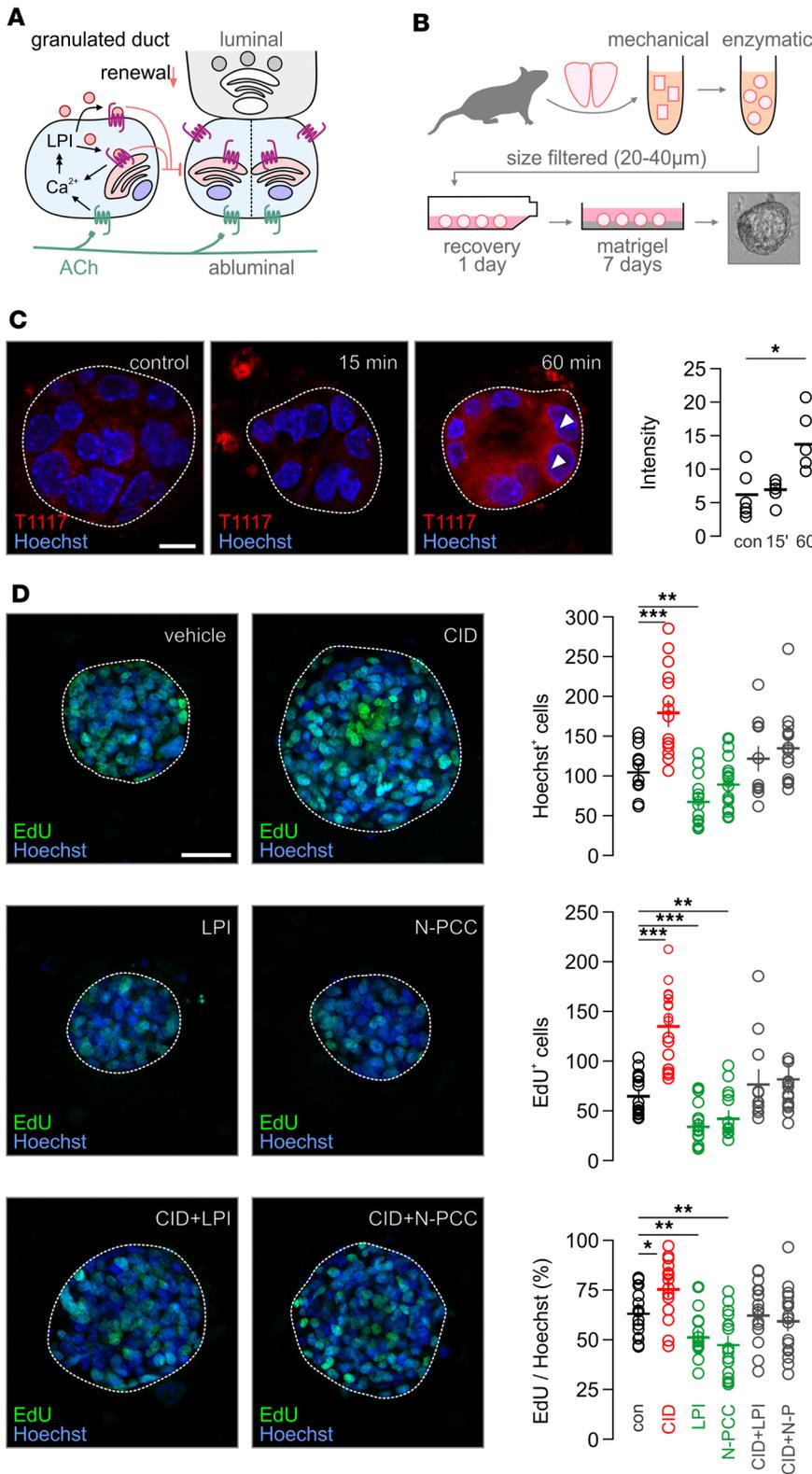
Figure 4. GPR55 negatively controls proliferation in cultured salispheres. (**A**) Schematic overview showing acetylcholine (ACh), released from parasympathetic terminals, promoting proliferation of abluminal epithelial cells. Simultaneously, ACh induces Ca^{2+} oscillations, leading to the synthesis of LPI through Ca^{2+}-dependent PLA2G4A. LPI then binds GPR55 through a predominantly autocrine process to prevent superfluous proliferation. Periodicity of cell division could be controlled by nerve activity and subsequent surges in LPI production. (**B**) Methodological description of salisphere cultures from mouse submandibular gland. (**C**) Feeding of T1117 results in significant signal accumulation after 1 hour (Student's t test). (**D**) Pharmacological manipulation of GPR55 signaling in size controlled salispheres (n = 10–15 clusters per group) leads to alterations in salisphere cell numbers and proliferation, as measured by EdU incorporation (1-way ANOVA). Scale bars: 20 μm (**C**), 10 μm (**D**). Data were expressed as means ± SEM. *$P <$ 0.05, **$P <$ 0.01, ***$P <$ 0.001.

if histochemical indices for altered glycoprotein metabolism are evident in *Gpr55*$^{-/-}$ mice, these are without atypical ductal cell swelling. Since ERp29 could be downregulated because of a change in ER size (40), we extended our findings to the ultrastructural level. Electron microscopy of *Gpr55*$^{-/-}$ ductal cells revealed strongly disrupted and reduced ER with frequent membrane blebbing, mostly flanked by the nucleus and compressed to the basal membrane (Figure 6F). Since GPR55 deletion results in diminished ER size and accumulation of glycoprotein, we postulate that, under physiological conditions, GPR55 activity could
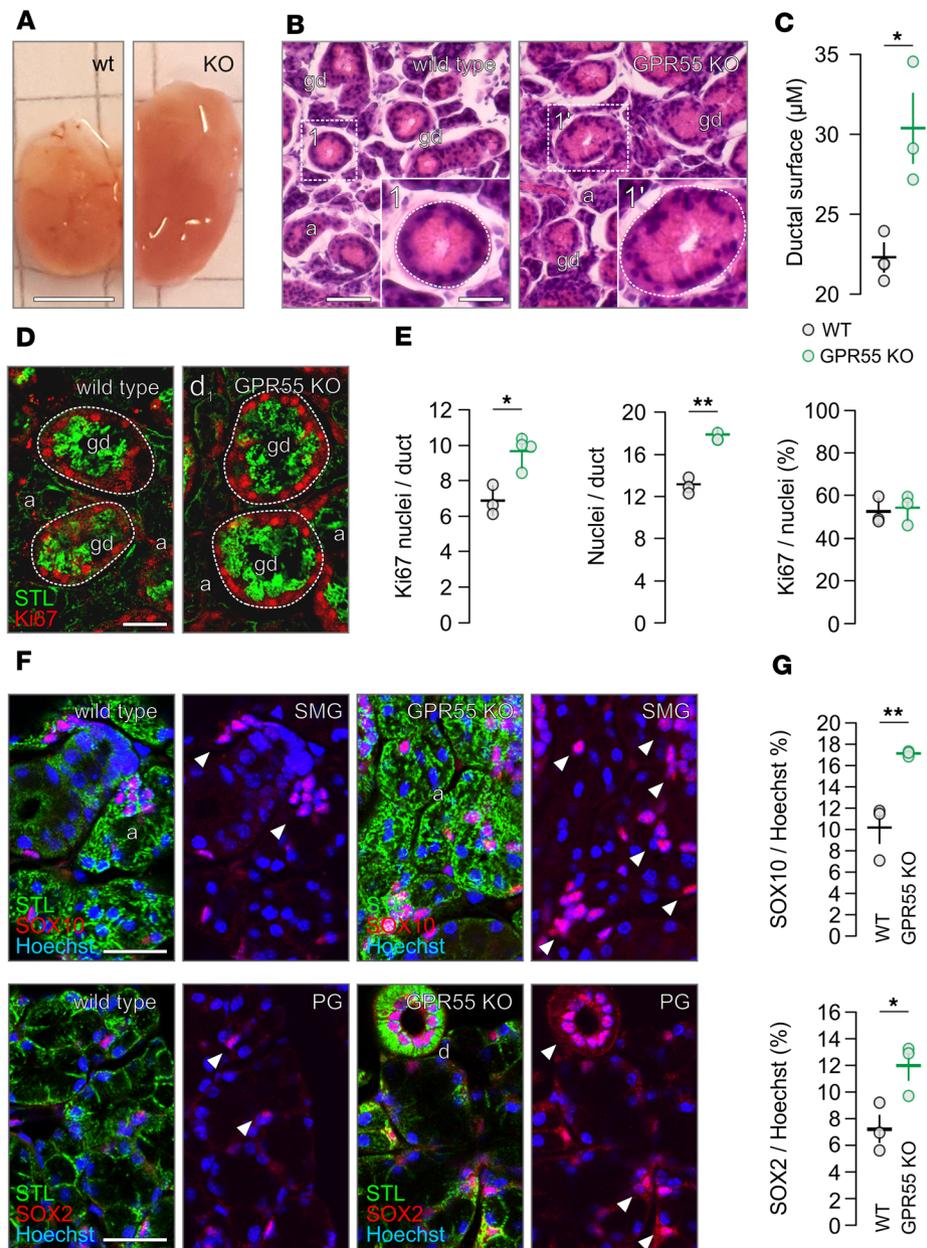
Figure 5. Increased submandibular gland proliferation in *Gpr55*⁻/⁻ mice. (**A**) Submandibular glands harvested from *Gpr55*⁻/⁻ animals were larger than their WT counterparts. (**B** and **C**) Hematoxylin analysis revealed enlarged granular ductal (gd) surface. (**D** and **E**) Staining for the proliferation marker Ki67 showed cell proliferation per granulated duct (*n* = 4–5 animals per group, Student's *t* test). (**F** and **G**) Similarly, the density of SOX10 and SOX2 immunreactive nuclei were found increased (arrowheads) in *Gpr55*⁻/⁻ submandibular and parotid glands, respectively, relative to WT controls. Scale bars: 5 mm (**A**), 50 μm (**F**), 25 μm (**B** and **D**). Data were expressed as means ± SEM. *P < 0.05, **P < 0.01.

also contribute to glycoprotein maturation, trans-Golgi trafficking, and release for salivation in mature granular duct cells (Figure 6G).

GPR55 antagonism promotes cellular maturation and glycoprotein synthesis in vitro. To confirm that dual-acting GPR55 could coincidently control both cellular maturation and glycoprotein synthesis, we applied CID 16020046 to primordial *tau2*-EGFP⁺/lectin⁺ salisphere stem cell clusters made up by 3–5 progenitors each (Figure 6H). Here, CID 16020046 significantly increased the number of clustered epithelial cells by day 5 in vitro (Figure 6I). Both the levels of EGFP (expressed by mature ductal cells) and glycoprotein (lectin⁺) were significantly elevated after CID 16020046 treatment (Figure 6I), indicating that GPR55 antagonism escalates the production of differentiated granular ductal cells. In contrast, LPI reduced cell survival (Figure 6I).
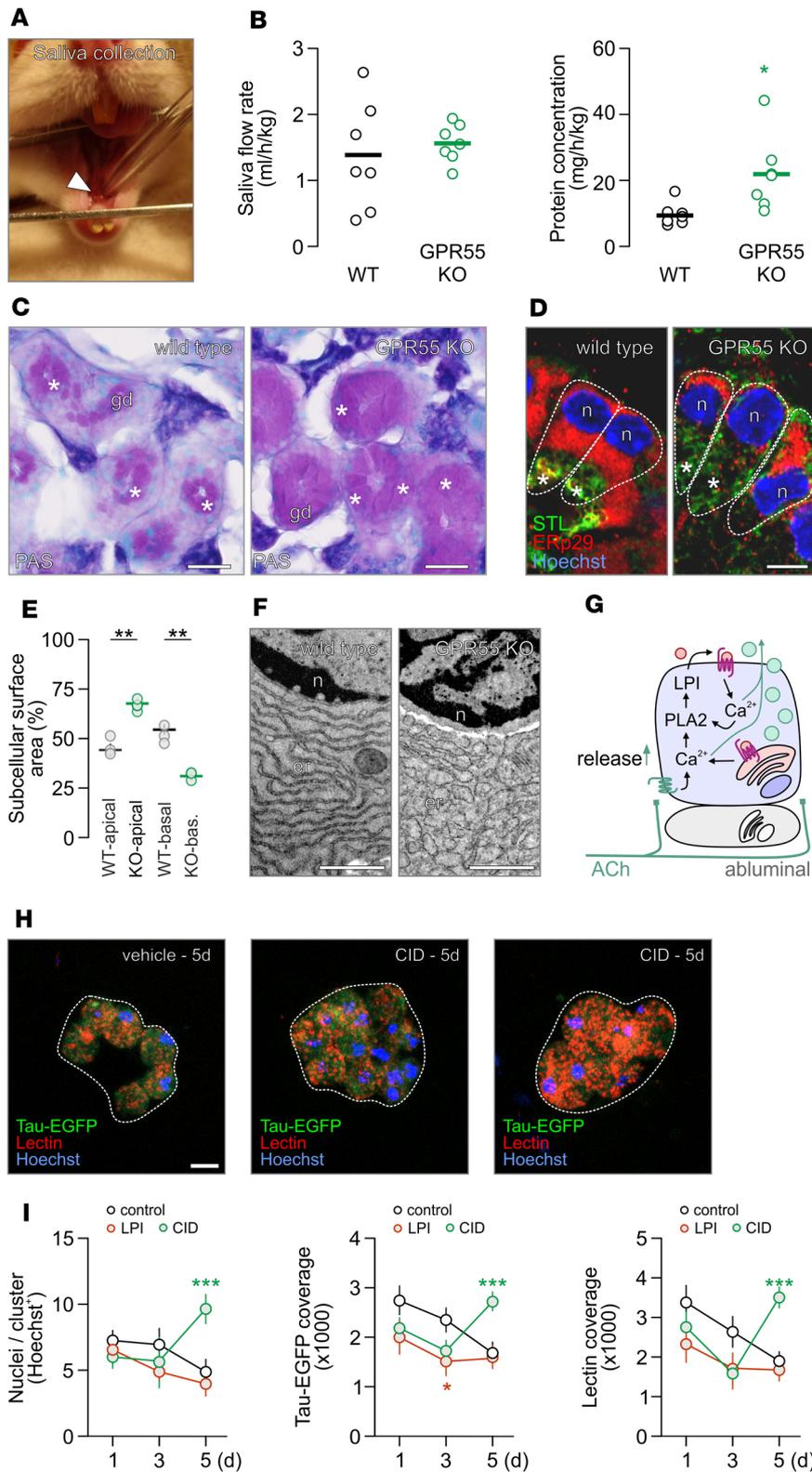
Figure 6. Excess glycoprotein production in *Gpr55*−/− mice. (**A**) We collected saliva with a flamed Pasteur pipette from the oral cavity in rodents (arrowhead). (**B**) Base salivary flow rate was unaffected in *Gpr55*−/− mice, while salivary protein content was significantly increased. (**C**) Periodic acid-Schiff reagent revealed glycoprotein accumulation in *Gpr55*−/− granulated ducts. Asterisks indicate compartmentalized glycoprotein accumulation. (**D** and **E**) Granulated ducts exhibit strongly reduced ERp29 immunolabeling in *Gpr55*−/− mice with enlarged apical release sites (Student's *t* test) Asterisks indicate compartmentalized glycoprotein accumulation. (**F**) Ultrastructural analysis of granulated ductal cells demonstrated reduced but swollen ER in *Gpr55*−/− mice (*n* = 3). (**G**) Schematic representation of a possible role for LPI-induced GPR55 signaling in salivation and glycoprotein release, in addition to limiting proliferation. (**H** and **I**) Exposure of small-cluster salispheres (3–5 cells) to CID 16020046 leads to proliferation, increased EGFP expression (*tau2*-EGFP), and glycoprotein accumulation (lectin) only after 5 days of treatment (*n* = 8–10 clusters per group; Student's *t* test). Note the worsening of cluster survival in LPI-treated salispheres. Scale bars: 50 μm (**C**), 10 μm (**D** and **H**), 1 μm (**F**). Data were expressed as means ± SEM. *$P < 0.05$, **$P < 0.01$, ***$P < 0.001$.

Conspicuously, cultured *Gpr55*−/− salispheres digested their seeding membrane matrix (Matrigel) in our in vitro model, while control salispheres remained attached. The digestion of the matrix, which could be rescued by application of surplus protein (10% FBS), implicates GPR55 in preventing the excess release of matrix-degrading enzymes (Supplemental Figure 5, I and J). Thus, we established an epithelial stem-to-granular ductal cell axis in which GPR55 is continuously expressed with its function spanning the control of the cell cycle and exocytosis.

GPR55 gates ACh-induced responses for salivation. Salivation is synergistically dependent on parasympathetic activity (ACh and norepinephrine release) and local peptide messengers (such as vasoactive intestinal polypeptide; ref. 41). Therefore, we tested if GPR55 activation could augment saliva production, particularly in physiologically mature ductal cells, for sufficiently long periods of time. Since intracellular $Ca^{2+}([Ca^{2+}]_iR)$ plays a key role in the release of protein and liquid components of saliva (42), and LPI signaling through GPR55 that couple to $G\alpha R_{12/13}R$ proteins can elevate $[Ca^{2+}]_iR$ (43, 44), we tested if GPR55 affects $[Ca^{2+}]_iR$ in salispheres. Fura-2 microfluorimetry was conducted in cells from *tau2*-EGFP (30) in which GFP selectively labels granular ductal cells (Supplemental Figure 2H). This helped to identify excretory luminal cells releasing glycoproteins. First, we applied ACh (5 μM), the neurotransmitter promoting salivation in vivo (8), and assigned Ca^{2+} responses in EGFP+ cells as maximal (e.g., 100% for quantification; Figure 7A). Subsequent superfusion of either LPI (3 μM) or N-PCC (1 μM) provoked low-amplitude Ca^{2+} oscillations after a 5-minute lag time (Figure 7, A and D). The mean amplitude of LPI- and N-PCC–induced transitory Ca^{2+} oscillations were around 9% and 14%, respectively, when normalized to the first ACh-induced Ca^{2+} spike (Figure 7D). Thus, the magnitude and timing of this response is reminiscent of $G\alpha R_{13}R$ signaling (43, 44). We then controlled for GPR55 involvement by showing that CID 16020046, an antagonist (3 μM; Figure 7, B and E), itself did not affect $[Ca^{2+}]_iR$ but occluded LPI-induced Ca^{2+} oscillations (at doses exceeding 3 μM).

Repeated ACh application leads to repetitive and slowly accommodating Ca^{2+} spikes in vitro (Figure 7C). Here, we used brief LPI pulses (up to 5 minutes) to avoid prolonged LPI-induced Ca^{2+} oscillations (Figure 7C vs. Figure 7A). Instead of accommodation, the second ACh-induced Ca^{2+} spike was augmented by LPI pretreatment (Figure 7, A and F), suggesting that agonist-induced GPR55 activation might be permissive for ACh-induced facilitated salivation in vivo (Figure 7G).

In *Gpr55$^{-/-}$* salispheres, both LPI and N-PCC failed to induce Ca^{2+} oscillations, confirming the specificity of our pharmacological tools in this particular biological setting. Notably, ACh superfusion resulted in Ca^{2+} transients, with significantly reduced amplitudes in *Gpr55$^{-/-}$* salispheres (Figure 7H), as compared with the responses of salispheres prepared from WT littermates. These data suggest that *Gpr55$^{-/-}$* salispheres remain immature even in adult mice, which is likely related to the expansion of tissue-resident progenitors (Figure 5, F and G).

To procure in vivo experimental support for GPR55's involvement in salivation in intact animals, we injected N-PCC (1 μM) into the mouse (Figure 7I) and rat (Supplemental Figure 6A) submandibular gland and collected saliva to measure salivation rate, as well as protein content. Injection of N-PCC (*n* = 4 mice, *n* = 6 rats) immediately and significantly increased salivation, as compared with vehicle controls (Figure 7I and Supplemental Figure 6A). Conversely, application of CID 16020046 alone (*n* = 4) significantly decreased salivation, while subsequent injections and N-PCC could not overcome the effects of CID 16020046 alone. Similarly, N-PCC was ineffective to increase salivation in *Gpr55$^{-/-}$* mice (Figure 7I). In addition, protein content in saliva collected after 10 minutes (or longer) of N-PCC treatment significantly increased (Figure 7I and Supplemental Figure 6B) in WT but not in *Gpr55$^{-/-}$* mice, suggesting that GPR55 activation engages the release of readily available saliva, as well as promotes de novo protein synthesis and release. Overall, we propose that GPR55 stimulation can induce Ca^{2+} release, at least in part, from intracellular stores (44) to maximize ACh responses that are essential for salivation.

Discussion

GPR55 receptors have generated significant interest recently as regulators of developmental processes (45) and pathologies (16, 46, 47), as well as phenomena associated with cell migration, subcellular motility, and amplification of signal transduction. Nevertheless, the physiological role of GPR55 in adult systems physiology remains unexpectedly obscure to this day, which we attribute to the often moderate-to-low levels of *Gpr55* expression (10). Here, we show *Gpr55* mRNA and protein expression in both human and mouse salivary glands at significant levels, together with enzymes critical for the production of its endogenous agonist, LPI. Since PLA2G4A is a Ca^{2+}-dependent enzyme and GPR55 agonism–elevates $[Ca^{2+}]_iR$, we outline a cell-autonomous amplification loop that is poised to transduce phasic responses upon parasympathetic stimulation (Figure 4A). Since ACh itself also raises $Ca^{2+}]_iR$ in ductal cells, we propose the existence of an ACh-LPI/PLA2G4A-GPR55 autocrine signaling axis, which exerts cell-type–specific actions (Figure 4A vs. Figure 6G). Given that Ca^{2+} is essential for both cell division/cell cycle progression, and vesicular release (48, 49), our results uncover a mode of dual regulation whose outcome is defined by cell
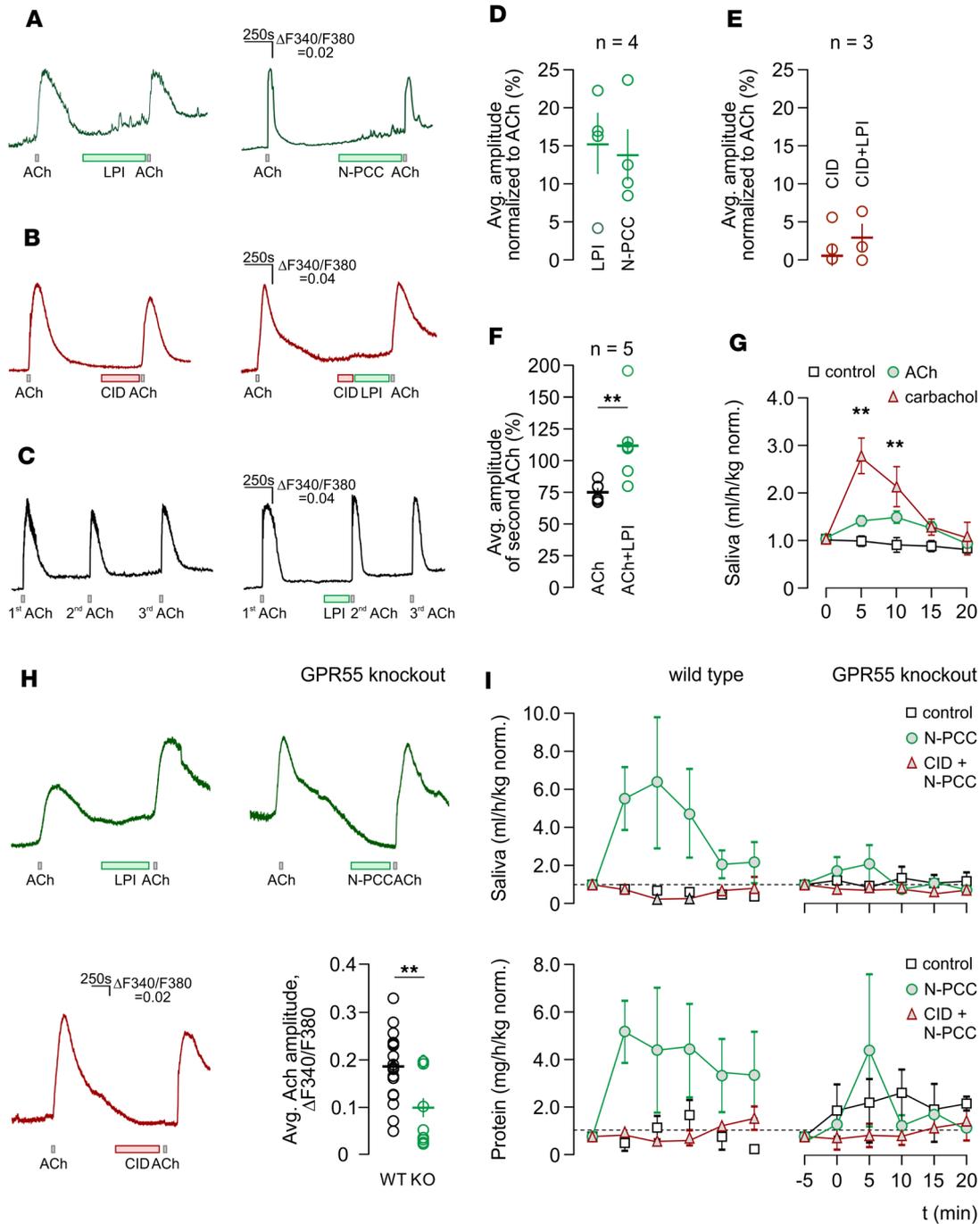
Figure 7. GPR55 signaling facilitates salivation. (**A** and **D**) GPR55 stimulation with LPI and N-PCC of salispheres induces delayed Ca²⁺ oscillations (*n* = 8–10 clusters per condition). (**B** and **E**) Inhibition of GPR55 signaling with CID has no effect alone but completely blocks LPI-induced Ca²⁺ oscillations. (**C** and **F**) LPI stimulation enhances the secondary ACh peaks (1-way ANOVA). (**G**) Intrasubmandibular injection of both ACh and carbachol induces salivation (*n* = 5–6 animals per condition). (**H**) LPI- and N-PCC–induced Ca²⁺ oscillations were absent in *Gpr55⁻/⁻* mice, with ACh responses almost halved compared with WT littermates. (**I**) Injection of N-PCC in the mouse submandibular gland leads to immediate salivation, which could be occluded by pretreatment with CID and is absent in *Gpr55⁻/⁻* mice (1-way ANOVA). (**I**) Total saliva protein content is increased after injection of N-PCC in WT mice but not in *Gpr55⁻/⁻* littermates. Data were expressed as means ± SEM. **P < 0.01.

state (e.g., allowing for differential recruitment of interacting proteins and signal transduction cascades) and physiological demands (Supplemental Methods on GPCR signaling).

The bulk of available literature recognizes GPR55 as a positive regulator of tumor growth, invasiveness, and worsened survivability (18). Here, we go significantly beyond these findings by showing

that GPR55 regulates physiological tissue renewal. Our hypothesis is supported by GPR55 being particularly highly expressed in self-renewing tissues, as compared with nonrenewing ones (10). Besides identifying myoepithelial cells flanking mucous acini as GPR55$^+$, we mechanistically tie GPR55 to slowing the cell cycle by using salispheres in vitro and *Gpr55$^{-/-}$* mice. From a clinical perspective, our data on mucoepidermoid carcinomas is important since these cancers arise from the transformation of myoepithelial cells physiologically expressing GPR55. The origin of this cancer phenotype might also explain the divergence of our data from existing concepts that incorporate an increase in GPR55 levels leading to ectopic gain-of-function upon tumorigenic transformation (18). Here, we show repression of GPR55 expression in tumor cells, which is instead compatible with deep deletion of *Gpr55* inducing salivary gland adenoid cystic carcinoma (50, 51) and anti-proliferative GPR55 action in cholangio-carcinoma (52). Thus, therapeutics of salivary gland cancers might benefit from reinstating GPR55 expression, augmenting LPI synthesis, and/or signaling to slow tumor progression. The finding that successful radiation therapy reinstates GPR55 levels might suggest that developing secondary therapies to help recovery after irradiation by topically activating GPR55 receptors could be effective to limit tumor remission. A tissue-specific aspect of our findings might be the reliance of salivary glands on nerve-induced autocrine LPI production, which generates temporal specificity for short-range LPI signaling. In the context of self-renewal, developmental processes are diversified by the availability of G proteins. Even though Gα are canonically thought to facilitate cell division, Gα subunits (e.g., Gα9) can also dampen signal responses through controlling cAMP levels (53). Alternatively, our data might be explained by a combination of constitutive GPR55 signaling with phasic agonist-induced receptor activation. Both mechanisms might mitigate known modulatory effects of GPR55 interactions with other GPCRs orchestrating cell proliferation (54, 55).

We also found GPR55 expressed on secretory granulated ductal cells, which are phenotypically mature excretory cells. When stimulated with LPI, Ca^{2+} oscillations ensue with a delay reminiscent of slower Gα$R_{12/13}$R-mediated signaling (56) observed previously in HEK293 cells (43, 44). This is in line with the finding that GPR55-mediated Ca^{2+} signaling is facilitated by RhoA/ROCK intermediate steps, leading to PLC activation, inositol triphosphate (IP3) production, and signaling at IP3 receptors on ER to drive Ca^{2+} release from intracellular stores. In addition, Ca^{2+}-induced Ca^{2+} release through ryonadine receptors potentiates GPR55 signaling (57), which also supports the lag time observed until engaging ER stores. The slowed response to LPI could also be explained by reliance on the Ca^{2+}-dependent activation of PLA2, priming the synthesis and accumulation of additional LPI. De novo–produced LPI could then engage even more GPR55, slowly building up to a Ca^{2+} crescendo and ultimately the release of glycoproteins. However, if GPR55 signaling is impaired and excretory cells become inactivated, then the intracellular sequestration of glycoproteins is likely to ensue. Indeed, we find enlarged pools of glycoprotein in *Gpr55$^{-/-}$* granular ductal cells, suggestive of glycoprotein retention. In parallel, high-resolution imaging at the light microscopy and ultrastructural levels revealed strongly disorganized ER, either due to compression through retention of release vesicles and/or the ER becoming dispensable to synthesize glycoprotein. This structural rearrangement of the ER in *Gpr55$^{-/-}$* cells is reminiscent of ER reorganization when B lymphocytes convert to plasma B cells and gain capacity to synthesize vast amounts of IgM multimers (40).

Overall, we uncovered unique roles for GPR55 in salivary glands that include the control of tissue regeneration and enhancement of functionality in mature excretory progenies. These findings are clinically relevant for xerostomia (dry mouth syndrome), a serious debilitating condition commonly associated with medication side effects (58) and illicit drug misuse (including cannabis and opioids), as well as salivary gland tumors, irradiation-induced tissue damage, and Sjögren's syndrome, an auto-immune disorder damaging salivary glands among other tissues (59). Regeneration of salivary tissue is therefore at the forefront of restorative medicine, with a focus on regrowing epithelium from stem cells for implantation (4). Our data suggest that topical application of GPR55 antagonists could radically limit the need for cell transplantation by their potency to increase innate proliferative capacity. A secondary benefit of focusing on GPR55 as a druggable target is the presumed lack of side effects on salivation. Likewise, enhancing GPR55 signaling by LPI-supplemented diets might become therapeutically appealing to limit tumorigenicity and tissue damage in salivary gland carcinomas.

Methods

Human tissue and histopathology. We collected human cases of epithelial-myoepithelial carcinoma ($n = 5$), mucoepidermoid carcinoma ($n = 5$), irradiated healthy glands (from head and neck pathologies) ($n = 5$), as well as healthy controls ($n = 5$) at the Medical University of Vienna. Tissues were obtained and used in accordance with the Declaration of Helsinki and compatible institutional guidelines. Extracted glands were fixed with 4% paraformaldehyde (PFA) for 2–5 days (Supplemental Table 1). Tissues were subsequently embedded in paraffin, cut at 4-μm thickness, and mounted on gelatin precoated glass slides (StarFrost). Pathology was verified on Hematoxylin-stained sections, while anatomical structures were identified by a combination of mucin staining (mucous acinar) and Hematoxylin counterstain (29).

Animal tissues and histology. Adult mice (C57BL/6J, *Gpr55^{-/-}* and *tau2*-EGFP; refs. 34, 30) were sedated with isoflurane (5%, 1 l/min flow rate) and subsequently killed by cervical dislocation. Submandibular glands were dissected and immersion fixed in 4% PFA in 0.01 M PBS (pH 7.4), while continuously agitated at 4°C overnight, and subsequently cryoprotected in 30% sucrose (in 0.0 M PBS) for at least 18 hours before being cryosectioned (Leica CM1850 UV) at 14-μm thickness onto electrically charged glass slides (SuperFrost Plus). For anatomical analysis, sections from *Gpr55^{-/-}* and WT mouse salivary glands were counterstained with H&E or processed for a standardized PAS (Leica) staining to visualize glycoprotein stores (including mucins).

Submandibular gland injections. Determination of salivation rate in vivo was performed on adult male Wistar rats with a body weight of 75–95 g ($n = 4$–6) and WT and *Gpr55^{-/-}* mice older than 3 months of age ($n = 9$ per genotype). Animals were anesthetized by an intramuscular bolus injection of ketamine (90 mg/kg body weight; Pharmac), as ketamine did not affect salivation in our protocols (data not shown). To collect saliva secreted by the submandibular gland, the 2 main ducts of both the right and left glands were cannulated with tightly closed flamed glass cannulae (diameter of the tip, 1.0–1.5 mm) in the oral cavity (Figure 6A). Saliva secreted over periods of 5 minutes (for 25 minutes total) was collected to evaluate salivation under unstimulated conditions and upon pharmacological treatment. Drug administration was carried out by intraglandular microinjection of 10 μl N-PCC (1 μM, Tapio Nevalainen) and CID 16020046 (10 μM, Tocris) in each glandular globe. Drugs were dissolved as stock solutions in DMSO and subsequently diluted in physiological saline. Salivation was measured as ml/hour/kg body weight–normalized outflow. Protein concentration (μg/ml) was determined with the Lowry protein assay (rat) and the NanoDrop 2000 (mouse). All values were normalized to baseline (t = –5)

IHC. Human salivary gland sections were stained overnight with antibodies as listed (Supplemental Table 3) and visualized for chromogenic detection by using DAKO's EnVision detection kit (Supplemental Methods), which amplifies reaction products upon horseradish peroxidase–driven conversion of DAB (in the presence of 0.05% H_2O_2 as substrate). Sections were counterstained with Mayer's hemalum solution (Merck). Sections from mouse submandibular glands were incubated with a cocktail of primary antibodies (Supplemental Table 3), visualized with fluorescent species–specific secondary antibodies (Jackson ImmunoResearch), and counterstained with Hoechst 33,342 (MilliporeSigma). Antibodies used include the following: Alexa Fluor 488 AffiniPure donkey anti–rabbit IgG (H+L, catalog 711-545-152), Alexa Fluor 488 Streptavidin (catalog 016-540-084), Cy3 AffiniPure donkey anti–rabbit IgG (H+L, catalog 711-165-152), Cy3 AffiniPure donkey anti–mouse IgG (H+L, catalog 715-165-151), Cy5 Streptavidin (catalog 016-170-084), Cy5 AffiniPure donkey anti–rat IgG (H+L, catalog 712-175-153), and Alexa Fluor 647 AffiniPure donkey anti–goat IgG (H+L, catalog 705-605-147). Fluorescent images were taken with an LSM 800 confocal microscope (Zeiss) and analyzed with ZEN software (Zeiss), while — for chromogenic immunostainings (human in situ and DAB stainings) — images of entire glass slides were captured and analyzed with a high-resolution digital slide scanner (NanoZoomer 2.0-HT, C9600-13, Hamamatsu Photonic) and NDP.view (Supplemental Methods). Requests for immunoreagents shall be addressed to KM.

Mouse salisphere cultures. To test GPR55 effects on cell proliferation, salispheres (Supplemental Methods) were treated alone or in combination with the GPR55 agonists LPI (1 μM; MilliporeSigma) (17) and N-PCC (100 nM), as well as the inverse agonist CID 16020046 (1 μM; Tocris) (33) 3 and 5 days after plating. EdU (5-Ethynyl-2'-deoxyuridine; 1 μM; MilliporeSigma) was simultaneously pulsed for 12 hours to label actively proliferating cells. Cells were washed once to remove excess EdU. On day 7, cultures were fixed with 4% PFA at 20°C–22°C and processed for immunocytochemistry and EdU Click-iT reactions (Thermo Fisher Scientific). Salispheres were kept no longer than 7 days in vitro since their growth slowed upon reaching a certain size (most likely due to limited nutrient availability to interior cells in larger clusters), possibly masking size differences at later time points. For Ca^{2+} imaging (Supplemental Methods), salispheres were used within 2–3 days after plating on Matrigel.

In situ hybridization. In situ hybridization was performed using PCR-derived digoxigenin–labeled riboprobes of the full coding sequence of mouse GPR55 (NM_001033290.2) according to published protocols (Supplemental Methods) (60). As negative control, adjacent sections were hybridized with a sense probe. For human tissues, hybridization was performed with digoxigenin-labeled riboprobes of the full coding sequence of the human GPR55 (NM_005683.3). Representative images were taken on an EVOS AMEX1000 microscope (Thermo Fisher Scientific).

PCR analysis. mRNAs were extracted from fresh submandibular glands using a SPLIT RNA extraction kit (Lexogen). mRNA (1 μg) was converted into cDNA using a High Capacity cDNA Reverse Transcription kit (Thermo Fisher Scientific) on a T100 thermal cycler (Bio-Rad) and was PCR amplified by mouse-specific primers (Supplemental Table 2). PCR products were resolved on 1.5% agarose gels to aid visual clarity and were imaged on a ChemiDoc XRS$^+$ system (Bio-Rad).

Electron microscopy. Electron microscopy was performed as previously published (61). Briefly, mouse submandibular glands from both WT and *Gpr55*$^{-/-}$ mice were dissected and immersion fixed in 4% PFA in 0.01 M PBS (pH 7.4) with continuous agitation at 4°C overnight. After repeated PBS washes, tissues were transferred into 30% sucrose for 18 hours, rapidly frozen on liquid NR_2R, and cryosectioned at 50-μm thickness (Leica CM1850 UV). Sections were osmificated (1% $OsOR_4R$ in 0.1 M PB [pH 7.4], 15 minutes), dehydrated in an ascending ethanol gradient, and flat-embedded in Durcupan (Fluka). Ultrathin sections (60 nm) were cut on a ultramicrotome (Leica Ultracut UCT), collected on single-slot formvar-coated grids, and analyzed by using a Tecnai 10 electron microscope (FEI; 15,000×).

Statistics. Results are presented as means ± SEM. Statistical analysis (Student's *t* test [2-tailed] or 1-way ANOVA as appropriate) was performed using GraphPad Prism 7 (GraphPad Software Inc.). A *P* value of < 0.05 was considered statistically significant. Graphs were constructed in GraphPad Prism 7, while figures were assembled in CorelDraw X7.

Study approval. Tissue collection from live animals conformed to the 2010/63/EU directive and was approved by the Austrian Ministry of Science and Research, Vienna (66.009/0145-WF/II/3b/2014 and 66.009/0277-WF/V/3b/2017) or the Indiana University Bloomington IACUC. Particular care was taken to minimize the number and suffering of experimental subjects. Human tissues were obtained and used in accordance with the Declaration of Helsinki and compatible institutional guidelines (Medical University of Vienna).

Author contributions

NF, EK, and TH conceived the study. SK, MIL, EB, JP, VC, and EK collected and analyzed data. NF, AJI, and KM contributed valuable tools and constructive criticisms. TH procured funding. EK and TH wrote the manuscript. All other authors commented on and approved submission of this manuscript.

Acknowledgments

Address correspondence to: Erik Keimpema, Department of Molecular Neurosciences, Center for Brain Research, Spitalgasse 4, A-1090, Vienna, Austria. Phone: 43.1.40400.31170; Email: erik.keimpema@meduniwien.ac.at.

1. Aure MH, Arany S, Ovitt CE. Salivary Glands: Stem Cells, Self-duplication, or Both? *J Dent Res*. 2015;94(11):1502–1507.
2. Pringle S, Van Os R, Coppes RP. Concise review: Adult salivary gland stem cells and a potential therapy for xerostomia. *Stem Cells*. 2013;31(4):613–619.
3. Hisatomi Y, et al. Flow cytometric isolation of endodermal progenitors from mouse salivary gland differentiate into hepatic and pancreatic lineages. *Hepatology*. 2004;39(3):667–675.
4. Nanduri LS, Maimets M, Pringle SA, van der Zwaag M, van Os RP, Coppes RP. Regeneration of irradiated salivary glands with stem cell marker expressing cells. *Radiother Oncol*. 2011;99(3):367–372.
5. Maimets M, et al. Long-Term In Vitro Expansion of Salivary Gland Stem Cells Driven by Wnt Signals. *Stem Cell Reports*.

2016;6(1):150–162.

6. Aure MH, Konieczny SF, Ovitt CE. Salivary gland homeostasis is maintained through acinar cell self-duplication. *Dev Cell*. 2015;33(2):231–237.

7. Knox SM, Lombaert IM, Reed X, Vitale-Cross L, Gutkind JS, Hoffman MP. Parasympathetic innervation maintains epithelial progenitor cells during salivary organogenesis. *Science*. 2010;329(5999):1645–1647.

8. Proctor GB, Carpenter GH. Regulation of salivary gland function by autonomic nerves. *Auton Neurosci*. 2007;133(1):3–18.

9. Sawzdargo M, et al. Identification and cloning of three novel human G protein-coupled receptor genes GPR52, PsiGPR53 and GPR55: GPR55 is extensively expressed in human brain. *Brain Res Mol Brain Res*. 1999;64(2):193–198.

10. Kremshofer J, Siwetz M, Berghold VM, Lang I, Huppertz B, Gauster M. A role for GPR55 in human placental venous endothelial cells. *Histochem Cell Biol*. 2015;144(1):49–58.

11. Moreno-Navarrete JM, et al. The L-α-lysophosphatidylinositol/GPR55 system and its potential role in human obesity. *Diabetes*. 2012;61(2):281–291.

12. Falasca M, Ferro R. Role of the lysophosphatidylinositol/GPR55 axis in cancer. *Adv Biol Regul*. 2016;60:88–93.

13. Pérez-Gómez E, et al. The orphan receptor GPR55 drives skin carcinogenesis and is upregulated in human squamous cell carcinomas. *Oncogene*. 2013;32(20):2534–2542.

14. Piñeiro R, Maffucci T, Falasca M. The putative cannabinoid receptor GPR55 defines a novel autocrine loop in cancer cell proliferation. *Oncogene*. 2011;30(2):142–152.

15. Ford LA, et al. A role for L-alpha-lysophosphatidylinositol and GPR55 in the modulation of migration, orientation and polarization of human breast cancer cells. *Br J Pharmacol*. 2010;160(3):762–771.

16. Kargl J, et al. GPR55 promotes migration and adhesion of colon cancer cells indicating a role in metastasis. *Br J Pharmacol*. 2016;173(1):142–154.

17. Oka S, Nakajima K, Yamashita A, Kishimoto S, Sugiura T. Identification of GPR55 as a lysophosphatidylinositol receptor. *Biochem Biophys Res Commun*. 2007;362(4):928–934.

18. Ross RA. L-α-lysophosphatidylinositol meets GPR55: a deadly relationship. *Trends Pharmacol Sci*. 2011;32(5):265–269.

19. Sutphen R, et al. Lysophospholipids are potential biomarkers of ovarian cancer. *Cancer Epidemiol Biomarkers Prev*. 2004;13(7):1185–1191.

20. Andradas C, et al. Activation of the orphan receptor GPR55 by lysophosphatidylinositol promotes metastasis in triple-negative breast cancer. *Oncotarget*. 2016;7(30):47565–47575.

21. Whyte LS, et al. The putative cannabinoid receptor GPR55 affects osteoclast function in vitro and bone mass in vivo. *Proc Natl Acad Sci USA*. 2009;106(38):16511–16516.

22. Romero-Zerbo SY, et al. A role for the putative cannabinoid receptor GPR55 in the islets of Langerhans. *J Endocrinol*. 2011;211(2):177–185.

23. Redman RS. On approaches to the functional restoration of salivary glands damaged by radiation therapy for head and neck cancer, with a review of related aspects of salivary gland morphology and development. *Biotech Histochem*. 2008;83(3-4):103–130.

24. Adams A, Warner K, Nör JE. Salivary gland cancer stem cells. *Oral Oncol*. 2013;49(9):845–853.

25. Yrjölä S, et al. Potent and selective N-(4-sulfamoylphenyl)thiourea-based GPR55 agonists. *Eur J Med Chem*. 2016;107:119–132.

26. Billah MM, Lapetina EG. Formation of lysophosphatidylinositol in platelets stimulated with thrombin or ionophore A23187. *J Biol Chem*. 1982;257(9):5196–5200.

27. Grzelczyk A, Gendaszewska-Darmach E. Novel bioactive glycerol-based lysophospholipids: new data -- new insight into their function. *Biochimie*. 2013;95(4):667–679.

28. Luz JM, Lennarz WJ. Protein disulfide isomerase: a multifunctional protein of the endoplasmic reticulum. *EXS*. 1996;77:97–117.

29. Palma SD, Simpson RHW, Skalova A, Leivo I. Major and Minor Salivary Glands. In: Cardesa A, Slootweg PJ, eds. *Pathology of the Head and Neck*. Berlin, Heidelberg, Germany: Springer; 2006:131–170.

30. Tucker KL, Meyer M, Barde YA. Neurotrophins are required for nerve growth during development. *Nat Neurosci*. 2001;4(1):29–37.

31. Daly CJ, Ross RA, Whyte J, Henstridge CM, Irving AJ, McGrath JC. Fluorescent ligand binding reveals heterogeneous distribution of adrenoceptors and 'cannabinoid-like' receptors in small arteries. *Br J Pharmacol*. 2010;159(4):787–796.

32. Drzazga A, Sowinska A, Krzeminska A, Rytczak P, Koziolkiewicz M, Gendaszewska-Darmach E. Lysophosphatidylcholine elicits intracellular calcium signaling in a GPR55-dependent manner. *Biochem Biophys Res Commun*. 2017;489(2):242–247.

33. Hofmann NA, et al. The GPR 55 agonist, L-α-lysophosphatidylinositol, mediates ovarian carcinoma cell-induced angiogenesis. *Br J Pharmacol*. 2015;172(16):4107–4118.

34. Wu CS, et al. GPR55, a G-protein coupled receptor for lysophosphatidylinositol, plays a role in motor coordination. *PLoS ONE*. 2013;8(4):e60314.

35. Gerdes J, Schwab U, Lemke H, Stein H. Production of a mouse monoclonal antibody reactive with a human nuclear antigen associated with cell proliferation. *Int J Cancer*. 1983;31(1):13–20.

36. Emmerson E, Knox SM. Salivary gland stem cells: A review of development, regeneration and cancer. *Genesis*. 2018;56(5):e23211.

37. Fernandes-Alnemri T, Litwack G, Alnemri ES. CPP32, a novel human apoptotic protein with homology to Caenorhabditis elegans cell death protein Ced-3 and mammalian interleukin-1 beta-converting enzyme. *J Biol Chem*. 1994;269(49):30761–30764.

38. Bebas P, Maksimiuk E, Gvakharia B, Cymborowski B, Giebultowicz JM. Circadian rhythm of glycoprotein secretion in the vas deferens of the moth, Spodoptera littoralis. *BMC Physiol*. 2002;2:15.

39. Mkrtchian S, Fang C, Hellman U, Ingelman-Sundberg M. A stress-inducible rat liver endoplasmic reticulum protein, ERp29. *Eur J Biochem*. 1998;251(1-2):304–313.

40. Federovitch CM, Ron D, Hampton RY. The dynamic ER: experimental approaches and current questions. *Curr Opin Cell Biol*. 2005;17(4):409–414.

41. Uddman R, Fahrenkrug J, Malm L, Alumets J, Håkanson R, Sundler F. Neuronal VIP in salivary glands: distribution and release. *Acta Physiol Scand*. 1980;110(1):31–38.

42. Ambudkar IS. Regulation of calcium in salivary gland secretion. *Crit Rev Oral Biol Med*. 2000;11(1):4–25.

43. Henstridge CM, Balenga NA, Ford LA, Ross RA, Waldhoer M, Irving AJ. The GPR55 ligand L-alpha-lysophosphatidylinositol

promotes RhoA-dependent Ca2+ signaling and NFAT activation. *FASEB J*. 2009;23(1):183–193.

44. Lauckner JE, Jensen JB, Chen HY, Lu HC, Hille B, Mackie K. GPR55 is a cannabinoid receptor that increases intracellular calcium and inhibits M current. *Proc Natl Acad Sci USA*. 2008;105(7):2699–2704.

45. Cherif H, et al. Role of GPR55 during Axon Growth and Target Innervation. *eNeuro*. 2015;2(5):ENEURO.0011-15.2015.

46. Celorrio M, et al. GPR55: A therapeutic target for Parkinson's disease? *Neuropharmacology*. 2017;125:319–332.

47. Staton PC, et al. The putative cannabinoid receptor GPR55 plays a role in mechanical hyperalgesia associated with inflammatory and neuropathic pain. *Pain*. 2008;139(1):225–236.

48. Pinto MC, et al. Calcium signaling and cell proliferation. *Cell Signal*. 2015;27(11):2139–2149.

49. Südhof TC. Calcium control of neurotransmitter release. *Cold Spring Harb Perspect Biol*. 2012;4(1):a011353.

50. Cerami E, et al. The cBio cancer genomics portal: an open platform for exploring multidimensional cancer genomics data. *Cancer Discov*. 2012;2(5):401–404.

51. Gao J, et al. Integrative analysis of complex cancer genomics and clinical profiles using the cBioPortal. *Sci Signal*. 2013;6(269):pl1.

52. Huang L, et al. Anandamide exerts its antiproliferative actions on cholangiocarcinoma by activation of the GPR55 receptor. *Lab Invest*. 2011;91(7):1007–1017.

53. Brzostowski JA, Johnson C, Kimmel AR. Galpha-mediated inhibition of developmental signal response. *Curr Biol*. 2002;12(14):1199–1208.

54. Martínez-Pinilla E, et al. CB1 and GPR55 receptors are co-expressed and form heteromers in rat and monkey striatum. *Exp Neurol*. 2014;261:44–52.

55. Moreno E, et al. Targeting CB2-GPR55 receptor heteromers modulates cancer cell signaling. *J Biol Chem*. 2014;289(32):21960–21972.

56. Singer WD, Miller RT, Sternweis PC. Purification and characterization of the alpha subunit of G13. *J Biol Chem*. 1994;269(31):19796–19802.

57. Yu J, et al. Differential activation of cultured neonatal cardiomyocytes by plasmalemmal versus intracellular G protein-coupled receptor 55. *J Biol Chem*. 2013;288(31):22481–22492.

58. Wolff A, et al. A Guide to Medications Inducing Salivary Gland Dysfunction, Xerostomia, and Subjective Sialorrhea: A Systematic Review Sponsored by the World Workshop on Oral Medicine VI. *Drugs R D*. 2017;17(1):1–28.

59. Generali E, Costanzo A, Mainetti C, Selmi C. Cutaneous and Mucosal Manifestations of Sjögren's Syndrome. *Clin Rev Allergy Immunol*. 2017;53(3):357–370.

60. Berghuis P, et al. Hardwiring the brain: endocannabinoids shape neuronal connectivity. *Science*. 2007;316(5828):1212–1216.

61. Malenczyk K, et al. A TRPV1-to-secretagogin regulatory axis controls pancreatic β-cell survival by modulating protein turnover. *EMBO J*. 2017;36(14):2107–2125.